In vitro detection and quantification of enamel and root caries using infrared photothermal radiometry and modulated luminescence

Raymond J. Jeon
Adam Hellen
Anna Matvienko
Andreas Mandelis
University of Toronto
Department of Mechanical and Industrial Engineering
Center for Advanced Diffusion-Wave Technologies
5 King's College Road
Toronto, Ontario, Canada M5S 3G8
E-mail: mandelis@mie.utoronto.ca

Stephen H. Abrams
Four Cell Consulting
Toronto, Ontario, Canada M3J 3G5

Bennett T. Amaechi
University of Texas Health Science Center at San Antonio
Department of Community Dentistry
Cariology Unit
San Antonio, Texas 78229

Abstract. Artificially created demineralized and remineralized carious lesions on the root and enamel of human teeth were examined by photothermal radiometry (PTR) and modulated luminescence (LUM). Fourteen extracted human teeth were used and a lesion was created on a 1 mm × 4 mm rectangular window, spanning root to enamel, using a lactic acid-based acidified gel to demineralize the tooth surface. The lesion was then exposed to a remineralization solution. Each sample was examined with PTR/LUM on the root and enamel before and after treatment at times from 1 to 10 (5 on root) days of demineralization and 2 to 10 days of remineralization. Ten-day (5 on root) demineralized samples were remineralized. After completing all the experiments, transverse microradiography (TMR) analysis was performed to compare and correlate the PTR/LUM signals to the depth of lesions and mineral losses. The PTR and LUM amplitudes and phases showed gradual and consistent changes with treatment time. In this study, TMR showed good correlation coefficients with PTR and LUM. It was also found that the length of the treatment time did not correlate very well to any technique, PTR/LUM or TMR, which implies a significant degree of inhomogeneity of the demireralization and remineralization rates in each and every tooth. [DOI: 10.1117/1.2942374]

Keywords: dental photothermal radiometry; modulated luminescence; root caries; demineralization and remineralization; thermal-wave interferometry.

Paper 07165R received May 7, 2007; revised manuscript received Dec. 17, 2007; accepted for publication Jan. 11, 2008; published online Jul. 1, 2008.

1 Introduction

Detection and monitoring of early carious lesions is becoming important in dental diagnostic research.[1–6] Early carious lesions that have just started to demineralize the underlying enamel crystal structure are not detectable by conventional visual diagnosis or dental radiographs.

In an effort to improve detection accuracy and use nonradiographic methods, lasers are considered promising for the early detection of carious lesions, mainly through the phenomenon of laser-induced fluorescence (or luminescence) of the enamel. The DIAGNOdent[7,8] is one such technology that is based upon the fluorescence caused by the porphyrins present in carious tissue and not on the amount of enamel demineralization.[9] A number of studies have been performed to assess the feasibility of using this instrument,[10–12] and it has been evaluated as having the potential to improve caries assessment in many ways. Tranæus et al.[6] recently reviewed three of these new methods—quantitative light-induced fluorescence (QLF), DIAGNOdent, and electronic caries monitor (ECM)—for caries detection and quantification. They concluded that these new techniques did not present enough evidence to be recommended as a substitute for traditional techniques, but the techniques might provide additional quantitative information for the evaluation of caries activity and risk assessment.

The first attempts to apply the depth profilometric capability of frequency-domain laser IR photothermal radiometry (PTR) toward the inspection of dental defects were reported by Mandelis et al.[13] and Nicolaides et al.[14] Some of the inherent advantages of the adaptation of this technique to the early detection of carious lesions in conjunction with modulated luminescence as a dual-probe technique also have been reported.[14–18] The PTR technique is based on the modulated thermal IR (blackbody or Planck radiation) response of a medium that results from optical radiation absorption of a low-power laser beam (~mW) and optical-to-thermal energy conversion, followed by a modulated temperature rise ("thermal waves") usually less than 1 °C in magnitude. The generated signals carry subsurface information in the form of a spatially damped temperature depth integral. In PTR applications to turbid media such as hard dental tissue, material property and depth information are obtained in two distinct modes: conductively from near-surface distances (~5 to 500 μm) controlled

Address all correspondence to Andreas Mandelis, Department of Mechanical and Industrial Engineering, University of Toronto, 5 King's College Road, Toronto, ON, Canada M5S 3G8; Tel.: 416/978–5106; Fax: 416/978–5106; E-mail: mandelis@mie.utoronto.ca

1083-3668/2008/13(3)/034025/11/$25.00 © 2008 SPIE

by the thermal diffusivity of enamel and the modulation frequency of the laser beam intensity; and radiatively through mid-IR blackbody emissions from considerably deeper regions commensurate with the optical penetration of the diffusely scattered laser optical field, a diffuse photon-density wave (several mm).[17,19] By optimizing the wavelength and modulation frequency of the PTR signal, one is able to examine and probe at least up to 5 mm below the enamel surface.[16] At low frequencies ($<$10 Hz), the conductive component of heat transfer usually dominates, whereas at high frequencies ($>$100 Hz), the radiative component becomes significant. From thermal-wave theory[20] it is well known that higher-frequency PTR signals contain information on near-surface phenomena, and full modulation frequency scans may be used to measure and reconstruct depth profiles of the relevant material properties, suchas the thermal diffusivity.[21] When used with dental materials, PTR has the ability to provide depth profilometric information on carious lesions.

The introduction of modulated (dynamic) luminescence (LUM) simultaneously with PTR[14,19] revealed the existence of two relaxation lifetimes originating in the hydroxyapatite composition of dental enamel. Variations in LUM emission fluxes and lifetimes between healthy and carious enamel were shown to have a limited depth profilometric character.[16,17] A combination of PTR and LUM has been developed into an analytical caries detection tool of combined specificity and sensitivity substantially better than the DIAGNOdent, radiographic, and visual methodologies.[16] Furthermore, PTR has been shown to have the potential to be a reliable noninvasive tool for the detection of early interproximal demineralized lesions that cannot be detected by conventional dental x-rays.[18]

The purpose of this study was to assess the ability of PTR and LUM to detect and monitor the degree of demineralization and remineralization of early-stage carious lesions on the root and enamel of human teeth. Lesions were artificially created by demineralization-remineralization agents with various treatment times and were scanned by PTR/LUM. These experimental results were compared with mineral loss and lesion depth, determined by the current "gold standard" for the measurement of mineral changes in tooth tissue: transverse microradiography (TMR). Correlation coefficients were calculated between the methods.

2 Materials and Methods

2.1 *Sample Preparation*

Fourteen extracted human teeth were used. Teeth were selected that had healthy surfaces and no visible defects, stains, restorations, or cracks. Each tooth was carefully cleaned with a tooth brush and polishing paste (Temrex), mounted on LEGO blocks [15.8 mm (W) × 15.8 mm (D) × 9.5 mm (H)], and stored in an air-tight humid container before measurements. The container consisted of two 90-mm-diam Petri dishes contacting each other rim-to-rim with a rubber band sealing off the circular contact interface. Inside this humid box, a small 35-mm-diam Petri dish was placed with distilled water to keep the ambient humidity constant. Mounting the teeth on LEGO blocks allowed the teeth to be separated and remounted into the same position during repeated measurements.

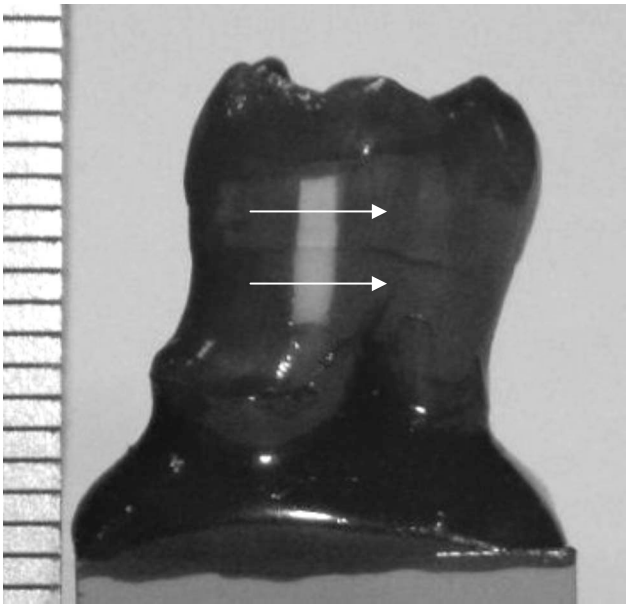

Fig. 1 Sample tooth on a LEGO brick coated with nail polish except for a 1 mm×4 mm window to treat. White arrows are shown where measurements were performed on the root and enamel.

Each sample was painted with two coats of acid-resistant polish except for a rectangular window [1 mm (W) × 4 mm (H)] extending from enamel to root as shown in Fig. 1. Demineralization or remineralization of each sample was carried out in 25 ml of treatment solution in a 50-ml polypropylene test tube, with the sample immersed upside down such that only the exposed rectangular window would be immersed in the solution. Demineralization to create a caries-like lesion was achieved by using an acidified gel system,[22] consisting of 0.1 M lactic acid solution gelled to a thick consistency with 6% w/v hydroxyethylcellulose (Aldrich, Dorset, UK) and the pH adjusted to 4.5 with 0.1 M NaOH. The remineralization solution[23] used in this study consisted of $MgCl_2 \cdot 6H_2O$ (0.03 g/L), K_2HPO_4 (0.121 g/L), KH_2PO_4(0.049 g/L), KCl (0.625 g/L), calcium lactate (3.85 g/L), fluoride (0.05 ppm), methyl-*p*-hydroxybenzoate (2.0 g/L), and sodium carboxymethylcellulose (0.4 g/L). The pH was adjusted to 6.7 using KOH. After treatment, samples were rinsed under running tap water for approximately 1 min and dried in air for 5 min. Following removal of the nail polish using acetone, each sample was again rinsed as above, dried, and stored in the air-tight box for at least 24 hours before measurement. Each sample was treated with a different demineralization and remineralization time period. Six samples were demineralized for up to 10 days for enamel and 5 days for root, then remineralized for 2, 5, and 10 days (two samples per time period). The remaining eight samples were demineralized for either 1, 2, 5 (both enamel and root), or 10 days (enamel only). Details of the sample treatment matrix are given in Table 1.

A sample tooth was taken out of the container before an experiment and was exposed to air for about 20 minutes for drying to avoid causing signal drift due to small humidity changes on the enamel surface. Then the tooth on the LEGO base was placed on the micropositioning stage, the laser was

Table 1 Sample treatment matrix.

Sample	Demineralization (day)							Remineralization (day)		
	1	2	3	4	5	8[a]	10[a]	2	5	10
R01	O	O	O	O	O	O	O	O	O	O
R02	O	O			O		O	O	O	O
R03	O	O			O		O	O	O	
R04	O	O			O		O	O	O	
R05	O	O			O		O	O		
R06	O	O			O		O	O		
R07	O	O			O		O			
R08	O	O			O		O			
R09	O	O			O					
R10	O	O			O					
R11	O	O								
R12	O	O								
R13	O									
R14	O									

[a]Enamel only.

O indicates when the PTR/LUM measurements were performed during treatment.

turned on, and another 10 minutes lapsed before measurements commenced so the sample surface would be thermally stabilized. As reported earlier,[17,18] after 20 minutes the effect of hydration on optical properties such as light scattering and fluorescence, as well as on thermal properties, is minimal or negligible for measurements lasting less than two hours.

2.2 *Experimental Apparatus and Procedures*

2.2.1 *PTR and LUM measurements*

The experimental setup is shown in Fig. 2. A semiconductor laser diode emitting at 659 nm (Mitsubishi ML101J27, maximum power 120 mW) was used as the source of both PTR and LUM signals. The diameter of the laser beam was approximately 150 μm. A diode laser driver (Thorlab, LDC 210) was used, triggered by the built-in function generator of the lock-in amplifier (EG&G 7265) to modulate the laser current harmonically. The modulated IR PTR signal from the tooth was collected and focused by two off-axis paraboloidal mirrors (Melles Griot 02POA017, rhodium coated) onto a mercury cadmium telluride (HgCdTe or MCT) detector (Judson Technologies J15D12, spectral range 2 to 12 μm, peak detectivity $D^* \approx 5 \times 10^{10}$ cm Hz$^{1/2}$ W^{-1} at ca. 12 μm). Before being sent to the lock-in amplifier, the PTR signal was amplified by a preamplifier (Judson Technologies PA-300). For the simultaneous measurement of PTR and LUM signals,

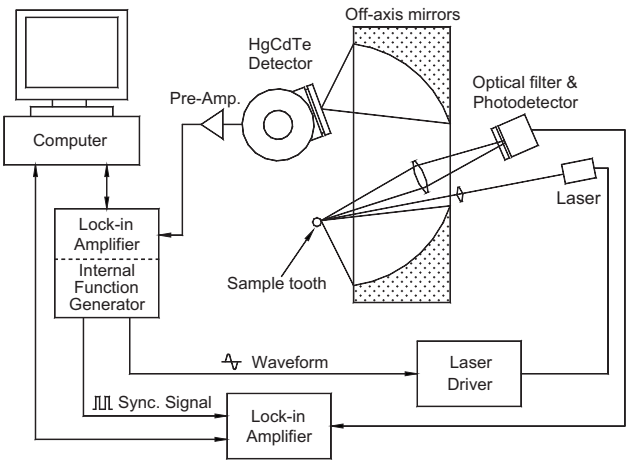

Fig. 2 Schematic diagram of PTR/LUM experimental setup.

a lens (focal length 100 mm) was placed above the off-axis paraboloidal mirrors where it did not block IR energy passage between the mirrors. The collected modulated luminescence was focused onto a silicon photodiode. A cut-on colored glass filter (Oriel 51345, cut-on wavelength 715 nm) was placed in front of the luminescence photodetector to block laser light reflected or scattered by the tooth. For monitoring the modulated luminescence, another lock-in amplifier (Stanford Research System, SR830) was used. Both lock-in amplifiers were connected to and controlled by a computer via RS-232 ports.

Two kinds of experiments were performed on both the enamel and root of each sample: (1) line scans in which the laser was scanned across the treated area of a tooth in the direction of the white arrows shown in Fig. 1 under normal incidence at fixed frequencies, 10 and 200 Hz; and (2) a frequency scan that measured the PTR and LUM signals at the center of each treated area (centers of the white arrows in Fig. 1) by varying the frequency from 1 Hz to 1 kHz. The frequency range was segmented into 25 equal intervals on a logarithmic scale by a data acquisition computer program, and the frequency was automatically incremented to the next value after each measurement. A 15-s time delay between measurements of the spatial coordinate scans allowed for thermalization of the tooth surface, that time interval being necessary to thermally stabilize the signals. Following completion of the PTR and LUM measurements, all samples were subjected to TMR analysis to determine the caries lesion parameters of mineral loss and lesion depth as described below.

2.2.2 *Transverse microradiography (TMR) and image analysis*

The samples were carefully sectioned using a water-cooled diamond-coated wire saw, model 3242 (Well, Le Locle, Switzerland), to produce an enamel slice approximately 100-μm thick from each lesion. These slices, together with an aluminum step wedge (10 steps of 24.5-μm thickness), were microradiographed on type 1A high-resolution glass x-ray plates (IMTECH CA, USA) with a Phillips x-ray generator system equipped with a nickel-filtered Cu-Kα target, which produced monochromatic radiation of a wavelength appropriate for hy-

droxyapatite (184 Å). The plates were exposed for 10 min at 20 kV/10 mA, then processed. Processing consisted of 5 min in a developer (Kodak HR) and 15-min in a rapid-fixer (Kodak) before a final 30-min wash period. After drying, the microradiographs were visualized using an optical microscope (Leica DMR) linked via a closed-circuit television camera (Sony, XC-75CE) to a computer (90-MHz Dell^{TM} Pentium). The enhanced image of the microradiograph was analyzed under standard conditions of light intensity and magnification, then processed, along with data from the image of the step wedge, using the TMR software (TMRW version 2.0.27.2, Inspektor Research Inc., Amsterdam, The Netherlands)[24] to quantify the lesion parameters of integrated mineral loss (Δz, vol% μm)and lesion depth (LD, μm). The mineral loss was computed as the difference in volume percent of mineral between sound and demineralized tissue integrated over the LD. The LD was assessed as the distance from the measured sound enamel surface to the location in the lesion at which the mineral content was larger than 95% of the mineral content in sound enamel. These were statistically compared and correlated to the PTR and LUM signals.

3 Results

Line-scan results on the root and the enamel of sample R01, which was demineralized sequentially from 1 to 10 days on enamel and 5 days on the root, then remineralized from 2 to 10 days, are shown in Figs. 3 and 4. Although measurements were performed after each treatment period as shown in Table 1, for clarity only five representative data sets—before treatment; after 1, 3, and 10 days on enamel (5 days on the root) of demineralization; and after 10 days of remineralization—are shown in the plots. All the samples listed in Table 1 exhibited consistent trends for all four signals (PTR and LUM, amplitudes and phases). In Figs. 3 and 4, the PTR amplitude showed a gradual increase with increasing demineralization time in the 1.5∼2.5-mm region, which had been exposed to the demineralization gel, then reversed direction (decreased slightly) after 10 days of remineralization. The PTR phase also exhibited gradual changes after each treatment as, shown in Figs. 3 and 4. At low frequency [10 Hz, Figs. 3(a) and 4(a)], the PTR phase lag for the root decreased throughout three days of demineralization, then reversed direction (started increasing) for the remainder of the demineralization-remineralization cycle. The PTR phase lag for the enamel kept on decreasing with longer demineralization times and reversed direction (started increasing) after the onset of the 10-day remineralization cycle. For both the root and enamel, the high-frequency PTR phase lag [200 Hz, Figs. 3(b) and 4(b)] increased with demineralization time and slightly reversed direction (decreased at the root) or remained essentially unchanged at the enamel. Comparing the LUM signals from the root and enamel, the LUM amplitude at 1.5 ∼2.5 mm from the enamel clearly decreased with respect to the unexposed baseline after 10 days of demineralization, while almost no change was observed in the root.

Figure 5 shows averaged signals within the treated region obtained from the line scans of Figs. 3 and 4. Putting the trends in those figures in perspective over the entire range of modulation frequencies, the PTR phases exhibit somewhat different trends between low and high frequencies from those at the same frequencies observed with the other three signal channels, which show similar trends. These differences can be understood in light of Fig. 6. Figures 6(a) and 6(b) show frequency scans at the center point of each treated region on the root and the enamel, respectively. The PTR amplitudes on both the root and enamel gradually increase with demineralization time over the entire frequency range, 1∼1,000 Hz. Figures 6(c) and 6(d) are normalized amplitude ratios (each curve is divided by the initial nontreated frequency scan as a reference) and phase differences (the initial nontreated phase scan is subtracted from each frequency curve), which are replotted from Figs. 6(a) and 6(b), respectively, to magnify the depth profilometric behavior of the PTR signals and details of the LUM signals.

Figure 7 shows the TMR images on the root and enamel of three representative samples, R01, R04, and R11, obtained following the PTR/LUM measurements. Figures 7(a) and 7(b) show two treated samples, R01 (10 days enamel, 5 days root-surface demineralization, and 10 days remineralization for both the enamel and root surface), and R04 (10 days enamel, 5 days root-surface demineralization, and 5 days remineralization for both the enamel and root surface). These figures clearly exhibit lesions on both the root and enamel. The TMR for sample R01 revealed integrated mineral loss of 1029.8 vol% μm on the enamel and 2219.3 vol% μm on the root, and the lesion depths were 66.7 μm in the enamel and 85.3 μm in the root, respectively. Sample R11, shown in Fig. 7(c), was demineralized for only two days, but the mineral loss on the root was 2631.0 vol% μm and the lesion depth was 89.9 μm, which were of similar magnitude to sample R01 (treated for 10 days), but much higher than sample R04.

The best correlation between TMR and PTR/LUM signals on root was obtained between the normalized PTR amplitude ratio versus mineral loss as measured with TMR, which yielded a correlation coefficient of 0.68, as shown in Fig. 8(a). Similarly, the best correlation on enamel was found between the normalized LUM amplitude ratio and the TMR lesion depth, with a correlation coefficient of −0.86 shown in Fig. 8(b). Specifically in the cases of samples R01 and R04, the cross-sectional enamel TMR images of Fig. 7 show a multilayer structure (a dark demineralized layer sandwiched between substrate and remineralized surface) following the demineralization-remineralization cycle.

4 Discussion and Conclusions

As described earlier and verified by TMR, subsurface lesions were artificially created on the root and enamel of human teeth by a demineralization gel and were subsequently reversed by a remineralization solution. The full cycle was examined by photothermal radiometry (PTR) and modulated luminescence (LUM). The PTR amplitude and phase in-line scans exhibited gradual and consistent changes with treatment time. Although LUM line scan signals showed less contrast over the lesions than PTR, both types of signals exhibited consistent changes with treatment time of individual teeth. The PTR phase line scans also exhibited high contrast for the created subsurface lesions with a stable baseline in the untreated region, and decreased phase lag at low frequencies. This is consistent with the higher scatter of the diffuse photon

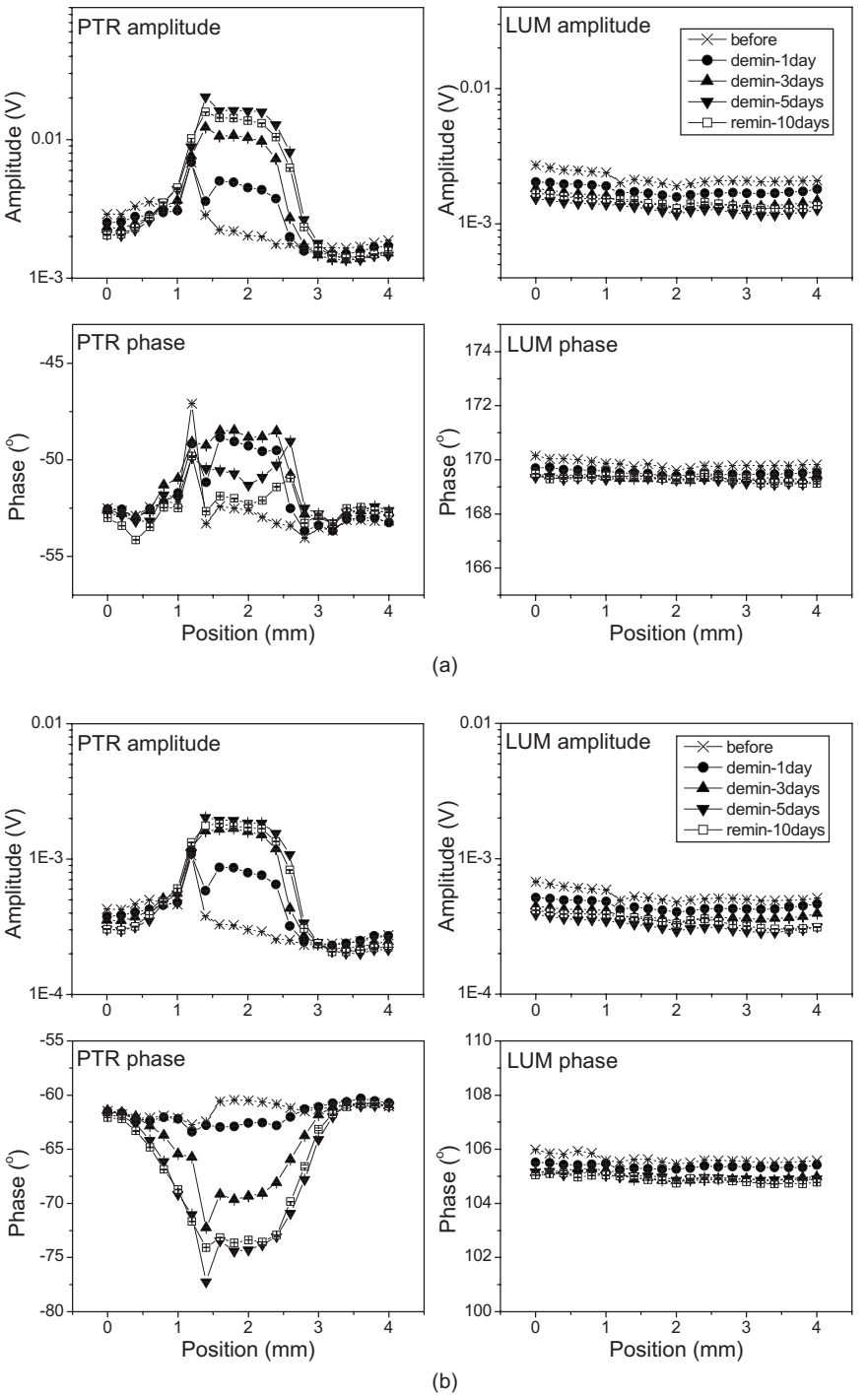

Fig. 3 Line scan results on the root of a tooth, R01, across the treated area at (a) 10 Hz, and (b) 200 Hz. Error bars, when not shown, are of the size of the symbols in these figures.

field and with thermal-wave confinement in the form of standing waves in the treated region, accompanied by decreased thermophysical properties (thermal diffusivity and thermal conductivity[20]). The LUM amplitude and phase show less contrast than their PTR counterparts, a fact consistent with previously reported studies on LUM.[16–18] It is important to note that there is a pronounced baseline drift of LUM amplitudes and phases within the coated (unexposed) region, unlike the steady PTR baseline. The LUM line scans, and consequently the frequency scans, showed a shifted baseline even in the region covered with nail polish and used as a reference, whereas PTR did not exhibit any measurable baseline drift away from the treated regions. This LUM behavior is consistent with our earlier observations and has been traced to the strong sensitivity of LUM signals to the degree of (de)hydration of teeth. Satellite experiments with deposition and etching off of nail polish on the untreated enamel revealed no signal changes as a function of duration and the number of

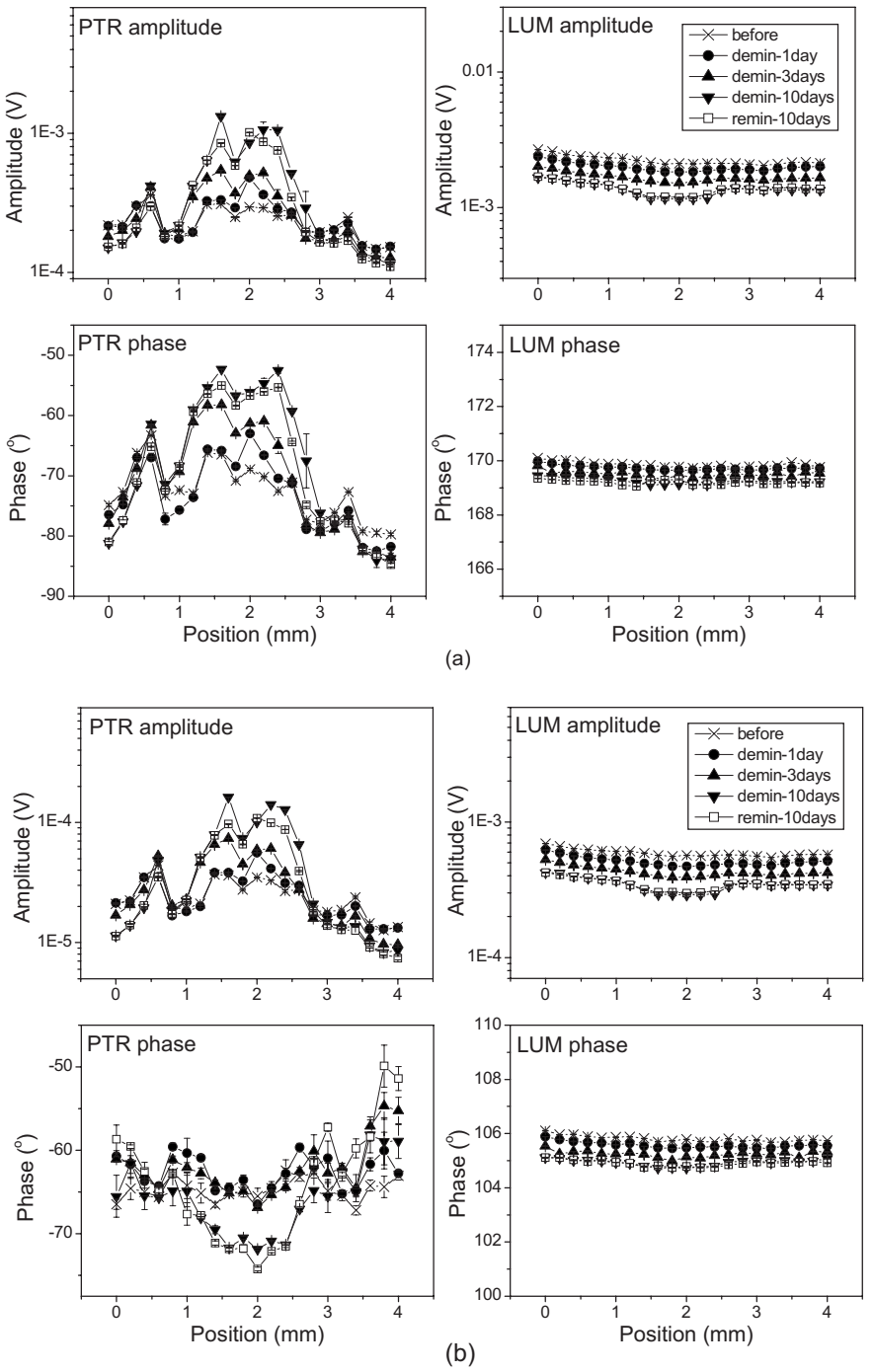

Fig. 4 Line scan results on the enamel of a tooth, R01, across the treated area at (a) 10 Hz, and (b) 200 Hz. Error bars, when not shown, are of the size of the symbols in these figures.

times the nail polish was painted on and etched off. Therefore, we concluded that the baseline shifts in Figs. 3 and 4 were not due to interactions between the tooth surface and nail polish. The overall degree of sensitivity of the LUM signals to demineralization is demonstrably inferior to PTR.

The PTR amplitude frequency scans in Fig. 6 showed clear indications of a depthwise growing lesion with a typically increasing amplitude and phase curvature.[16] The relatively higher PTR amplitude on the treated area than its neighboring untreated region is typical behavior of PTR amplitudes in cases of natural caries, defects on the tooth surface such as a stain or a crack, or demineralized enamel, as reported in our earlier studies.[16–18] It should be noted that the PTR amplitude curves after demineralization exhibited the onset of curvature in the middle of the frequency range. This is typical of PTR amplitude in the presence of carious lesions, as shown in an earlier study.[16] It is related to the onset of thermal-wave interference within the enamel/root demineralized surface layer, a layer growing in thickness during demineralization, with different optical absorption and scattering properties, as well as

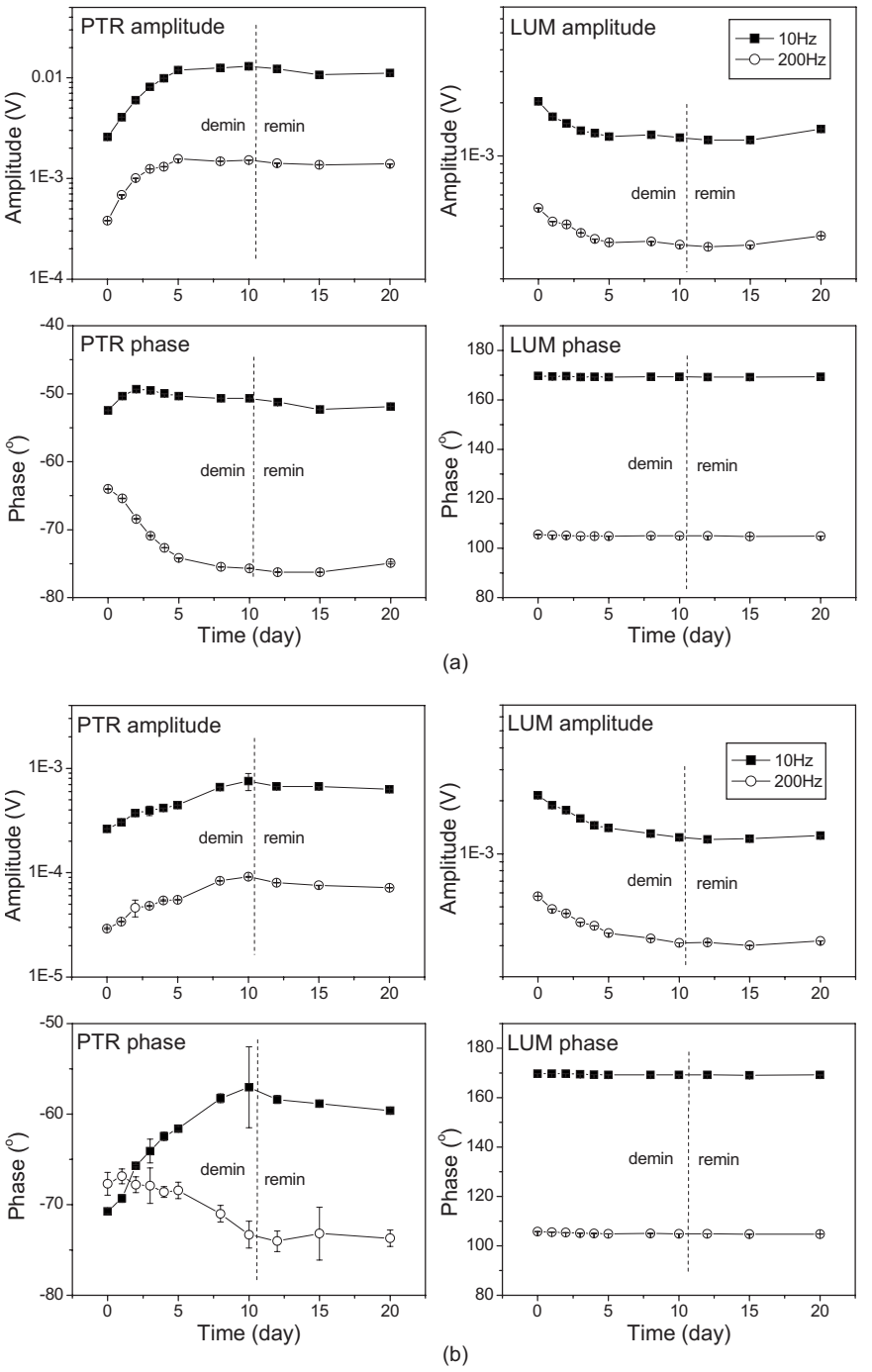

Fig. 5 PTR/LUM signal kinetics vs. treatment time at 10 and 200 Hz on (a) root, and (b) enamel of a tooth, R01. Error bars, when not shown, are of the size of the symbols in these figures.

different thermophysical properties from untreated enamel or root. After 10 days of remineralization, the PTR root amplitude exhibited a slight decrease throughout the entire frequency range above 5 Hz, a sign of the onset of a thin surface layer of mineral recovery, as verified by TMR. However, on the enamel, the PTR amplitude [Fig. 6(b)] increased only slightly in the entire low-frequency range below approximately 100 Hz. This slow response to the remineralization solution may occur because it is more difficult for enamel to remineralize than root at relatively short remineralization times. Very remarkable features of the phase curves are the crossovers at intermediate frequencies. The PTR phase curves in Figs. 6(a) and 6(b) demonstrate a very sensitive signal channel that shows evidence of a growing demineralization overlayer; a larger phase lag at low frequencies in the untreated tooth is due to the relatively low-incident photon scattering, which allows a longer optical attenuation depth and larger phase lag of the generated photothermal response.[19] The shift of the inflection point of the phase to lower frequency with increasing demineralization is also consistent

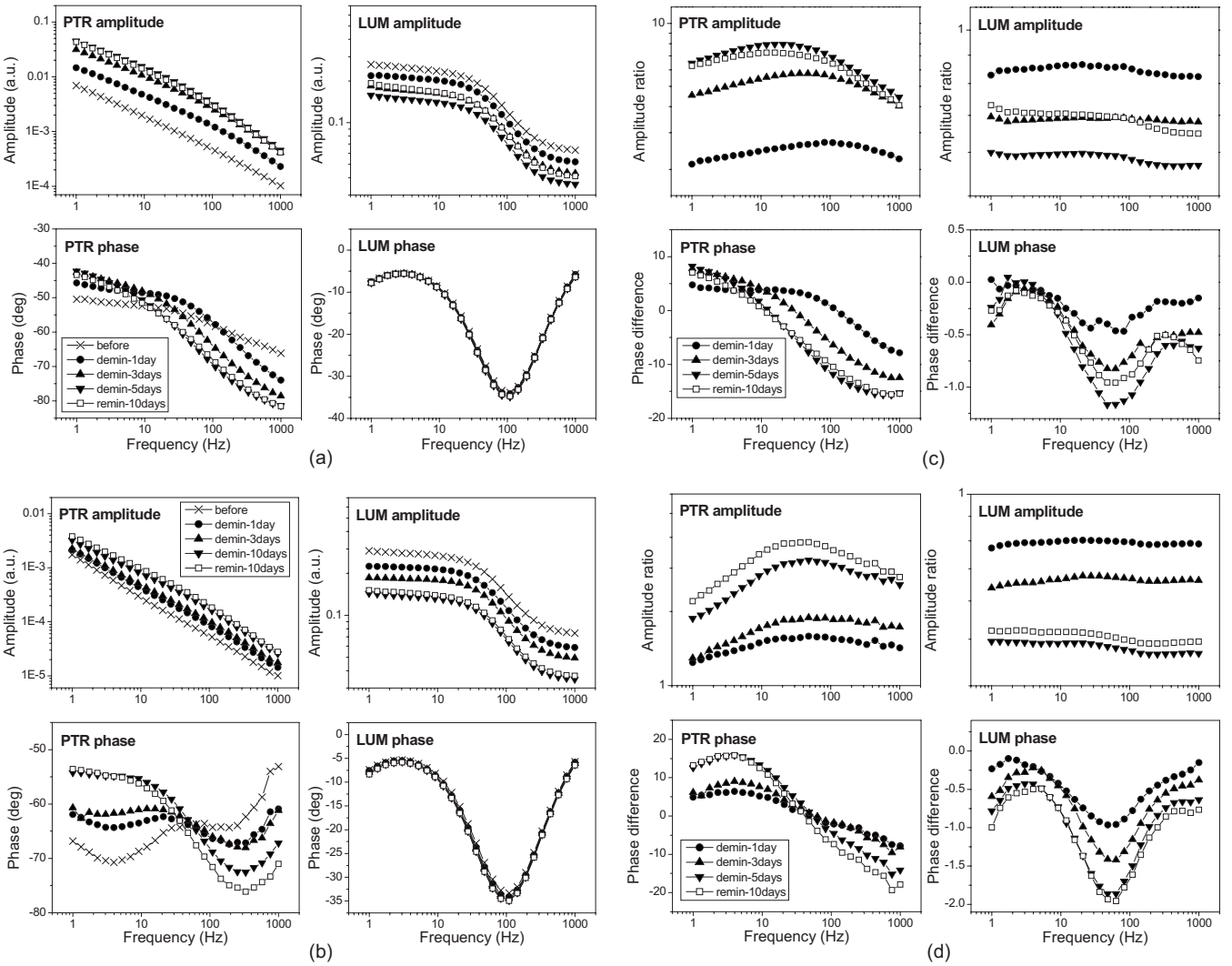

Fig. 6 Frequency-scan results of a tooth, R01, at the center of the treated area from 1 to 1,000 Hz on (a) root, and (b) enamel. Amplitude ratio and phase difference of each curve with respect to the initial state (before treatment) on (c) root, and (d) enamel.

with a thicker surface layer and/or poorer (decreased values of) thermal diffusivity of the layer.[20]

After 10-day remineralization, the LUM amplitude increased for both the root and enamel, as shown in Figs. 6(a) and 6(d). The increase of the LUM amplitude on the root was much larger than that on the enamel [Figs. 6(c) and 6(d)], which is also consistent with trends in the PTR signal amplitude changes. A signal reversal amplification factor in LUM may be a combination of enamel recrystallization and decreased water diffusion in the hydroxyapatite microstructure during the remineralization process, which yields a higher sensitivity of the LUM amplitude to remineralization than that expected from each individual process acting independently. Small but measurable, high signal-to-noise ratio (SNR) LUM phase changes have been observed for both root and enamel. In Figs. 6(c) and 6(d), frequency-scan normalized PTR amplitude and phase extrema and inflection points show clear evidence of standing thermal-wave interference patterns in the presence of a growing overlayer of different optical and thermal properties from the substrate.[20] The maximum amplitude of each PTR curve from the root tends to move to a lower frequency with increased demineralization time [Fig. 6(c)], which indicates the interface between the demineralized root surface and intact substrate recedes away from the surface with longer demineralization time. Following the onset of remineralization, the maximum of the normalized amplitude shifts to a slightly higher frequency, an indication of a change in the evolution of the surface thin layer. As already mentioned in conjunction with Figs. 6(a) and 6(b), the inflection points of the demineralization PTR phase curves on the root in Fig. 6(c) also show monotonic shifts toward lower frequency, and a reversal in the case of the remineralized curve. Therefore, both PTR signal channels point to depth profilometric behavior in the sense that during demineralization, they are dominated by a growing surface layer of thickness commensurate with the thermal diffusion length in the layer.[20] This condition generates the amplitude maxima and phase inflection points. Indeed, the range of known thermal diffusivity, α; values of healthy dental enamel, 4.2×10^{-7} m^2/s (Ref. 25) to 4.69×10^{-7} m^2/s (Ref. 26); and the average frequency of the phase inflection points in enamel in Figs. 6(b) and 6(d)

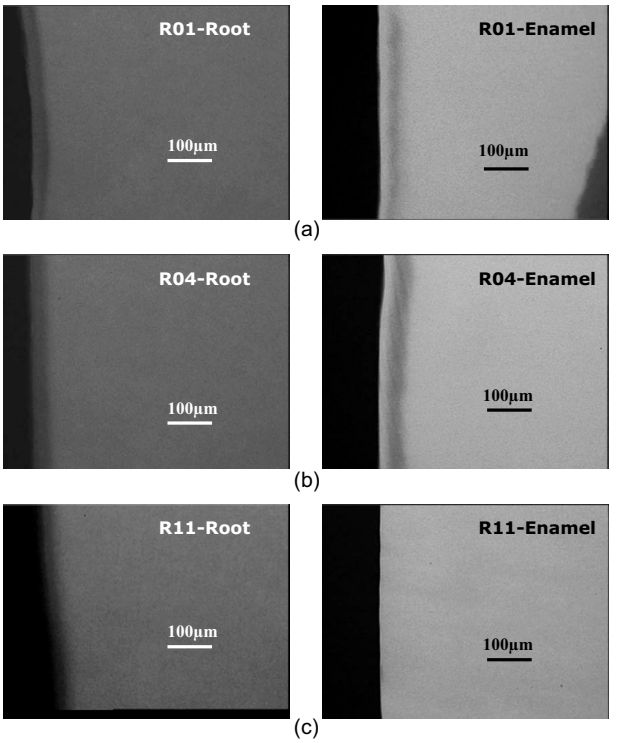

Fig. 7 TMR cross-sectional images of (a) the 10-day (5-day on root, left) demineralized and 10-day remineralized sample, R01; (b) the 10-day (5-day on root, left) demineralized and 5-day remineralized sample, R04; and (c) the 2-day demineralized sample, R11 (root on left).

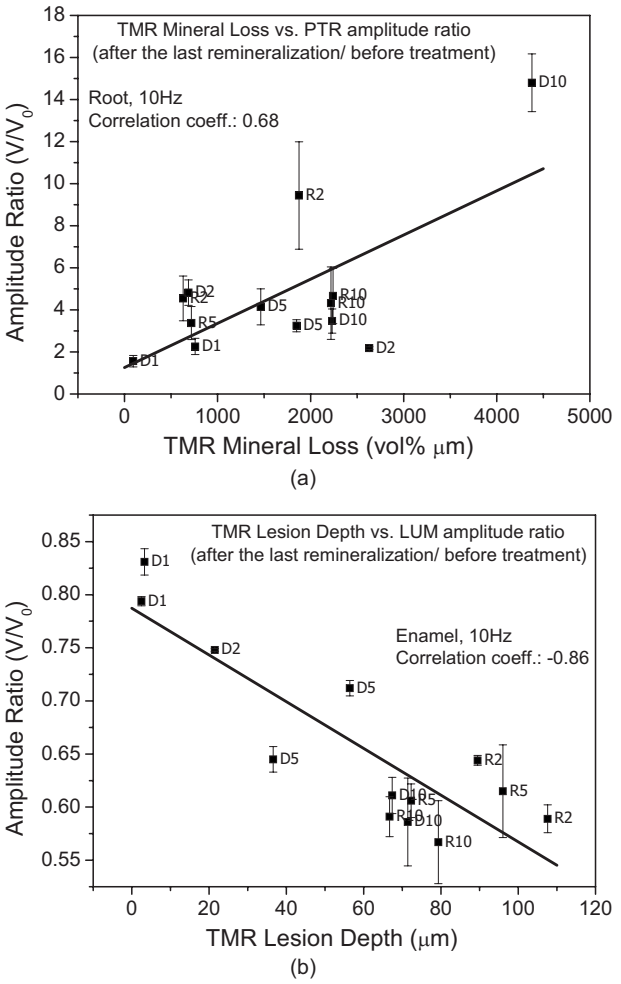

Fig. 8 Correlation between (a) PTR amplitude ratio and TMR mineral loss on root; and (b) LUM amplitude ratio and TMR lesion depth on enamel. The number on the right of each datum represents days of treatment with a leading letter D for demineralization and R for remineralization. V and V_0 stand for the amplitude after the last remineralization and the amplitude before treatment, respectively.

($f \sim 50$ Hz)and that of the amplitude ratio maximum in Fig. 6(d) can be used to devise an equation for the thermal diffusion length:

$$\mu(f) = \sqrt{\alpha/\pi f}. \quad (1)$$

Using Eq. (1), one finds $\mu(50\ \text{Hz}) \sim 51.7$ to 54.6 μm, values that are consistent with the demineralization layer thickness scale shown in Fig. 7. The thermal diffusivity of demineralized dental enamel has not been reported to our best knowledge; however, we expect it to be somewhat lower than that of healthy enamel, which would shrink the diffusion length somewhat, but in the same general thickness range as the healthy counterpart. Similar arguments apply to the case of the thermal properties of the dental root.

However, in the enamel data shown in Fig. 6(d), those PTR maxima and inflection-point shifts are much reduced, as discussed in conjunction with Figs. 6(a) and 6(b). This may be interpreted as a less-effective overlayer growth on the enamel than on the root, a fact borne out by TMR depth profilometric measurements. Furthermore, in an enhancement of the trends in Figs. 6(a) and 6(b), the normalized amplitudes and phases clearly exhibit the aforementioned monotonic behavior, even after the onset of remineralization. The low-frequency amplitude (contributions from deeper subsurface regions) shifts the most with a decreasing shift toward the high frequencies. This trend is indicative of near-surface restoration of the state of the enamel prior to demineralization. In this three-layer configuration, the monotonic amplitude increase during the remineralization phase is the result of enhanced thermal-wave confinement within the subsurface demineralized layer [Fig. 7(a)], which is now thinner and thus maintains a higher mean oscillating temperature. At high frequencies, however, the reduced thermal diffusion length becomes commensurate with the thickness of the demineralized layer, which is much larger than the remineralized surface layer. Therefore, the PTR amplitude converges to that of the five-day demineralized configuration. This hypothesis is also supported by the TMR cross-sectional images in Fig. 7(a).

On the other hand, LUM amplitudes are not indicative of optical interferometric behavior for either the root or enamel. The absence of such behavior is due to three factors: (1) the dental media are turbid, and as such, they strongly scatter the laser light and prevent the formation of an optical standing-wave pattern; (2) the demineralized layer-substrate interface is not sharp enough to generate significant reflection intensity to produce an interference pattern; and (3) the thickness of the demineralized layer is too large compared to the wavelength of the light.

The normalized LUM phases exhibit the well-known minimum due to an optical relaxation time characteristic of hydroxyapatite[14] and show very well-resolved shifts from the untreated baseline scans on the root [Fig. 6(c)] and on the enamel [Fig. 6(d)]. The high SNR allows observation of the evolution of the minima at approximately 60 Hz during the demineralization phase, followed by reversal in the root after 10 days of remineralization, but with no reversal in the enamel. Unlike the PTR phases, the LUM phase frequency scans have the disadvantage of not being entirely independent of baseline shifts, as shown in Figs. 3 and 4. Therefore, in general it is difficult to deconvolute the true shift due to the overlayer thickness from the baseline drift effects. Nevertheless, unlike the amplitude ratios, the LUM phase differences are less sensitive to the overlayer growth in frequency ranges well outside the optical relaxation rate range (~10 to 300 Hz), which controls the minimum,[15] as shown in Figs. 6(c) and 6(d). As a result, the relative trends in the LUM phases of Figs. 6(c) and 6(d) are measurably sensitive to overlayer thickness evolution in the 10 to 300 Hz range and can be used to corroborate the concurrent PTR trends, as discussed above. This is evident from the relative shifts in the phase minima and reversal of the remineralized curve in the root-surface [Fig. 6(c)], while an absence of reversal is seen in the enamel [Fig. 6(d)]. The PTR/LUM line and frequency scans from other samples exhibited similar general behavior to sample R01 and will not be presented here. The higher mineral loss and deeper lesion depth at the root are consistent with the higher resistance of enamel to demineralization by acid and the more pronounced thermal-wave interferometric behavior at the root in Figs. 6(a) and 6(d). However, as shown in Table 2, some tooth samples showed opposite results. For example, R04 shown in Fig. 7(b) exhibited a higher mineral loss and deeper lesion depth on the enamel than on the root. Therefore, it was clearly established that the treatment duration with the artificial caries solution did not correlate with the extent and severity of lesions as measured by the mineral-loss-sensitive TMR technique. It was equally difficult to find a correlation between the PTR/LUM signals and treatment time. This is because the rate of demineralization andremineralization can vary greatly among teeth, between surfaces on the same tooth, and even between sites on the same surface of a tooth.[22] This has also been observed in a recent PTR/LUM study.[18] The interface between surface layers and substrate in the enamel images is more diffuse than that at the root, an observation that is consistent with the more pronounced thermal-wave interferometric pattern from the root (Fig. 6). A detailed photothermal model of the multilayer structure is currently under consideration.[27]

In view of the good correlation of PTR/LUM with the mineral loss or the lesion depth measured with TMR results, it can be concluded that PTR/LUM is capable of monitoring artificially created carious lesions, their evolution during demineralization, and the reversal of the lesions under the growth of a remineralized surface layer. It was also found that cumulative treatment time did not correlate well with either PTR/LUM or TMR, which is indicative of significant variations in demineralization-remineralization rates among different teeth as well as across each individual tooth.

Table 2 Mineral losses and lesion depths measured by TMR.

		TMR			
		Enamel		Root	
Sample	Treatment (demin. days-remin. days)	Mineral loss (vol% μm)	Lesion depth (μm)	Mineral loss (vol% μm)	Lesion depth (μm)
R01	D10[a]-R10	1029.8	66.7	2219.3	85.3
R02	D10[a]-R10	1422.7	79.3	2240.6	126.0
R03	D10[a]-R5	2236.6	96.0	-	-
R04	D10[a]-R5	1385.8	72.3	718.6	48.0
R05	D10[a]-R2	2282.2	89.5	629.9	35.3
R06	D10[a]-R2	2864.2	107.6	1875.4	68.9
R07	D10[a]	1483.1	71.4	2230.2	70.1
R08	D10[a]	924.4	67.4	4377.9	114.0
R09	D5	257.1	36.6	1464.2	58.8
R10	D5	637.4	56.4	1848.6	64.4
R11	D2	175.8	21.5	2631.0	89.9
R12	D2	-	-	687.6	50.0
R13	Dl	52.8	3.3	94.6	9.5
R14	Dl	55.8	2.5	758.8	65.4

[a]D5 on roots.

Acknowledgments

The support of the Ontario Centres of Excellence (OCE)–Materials and Manufacturing Ontario (MMO) with a collaborative contract, of the Natural Sciences and Engineering Research Council (NSERC), and of Four Cell Consulting is gratefully acknowledged.

References

1. G. N. Jenkins, "Recent changes in dental caries," *Br. Med. J.* **291**, 1297–1298 (1985).
2. D. Ricketts, E. Kidd, K. Weerheijm, and H. de Soet, "Hidden caries: What is it? Does it exist? Does it matter?" *Int. Dent. J.* **47**, 259–265 (1997).
3. D. McComb and L. E. Tarn, "Diagnosis of occlusal caries: Part I. conventional methods," *J. Can. Dent. Assoc.* **67**, 454–457 (2001).
4. K. J. Anusavice, "Need for early detection of caries lesions," in *A United States Perspective in Early Detection of Dental Caries II, Proc. 4th Annual Indiana Conf.*, G. Stookey, Ed., pp. 13–30 (2001).
5. A. F. Zandoná, "Diagnostic tools for early caries detection," *J. Am. Dent. Assoc.* **137**, 1675–1684 (2006).
6. S. Tranæus, X.-Q. Shi, and B. Angmar-Månsson, "Caries risk assessment: methods available to clinicians for caries detection." *Community Dent. Oral Epidemiol.* **33**, 265–273 (2005).
7. R. Hibst and K. Konig, "Device for detecting dental caries," U.S. Patent No. 5,306,144 (1994).
8. R. Hibst, R. Gall, and M. Klafke, "Device for the recognition of caries, plaque or bacterial infection on teeth," U.S. Patent No. 6,024,562 (2000).
9. H. M. Alwas-Danowska, A. J. M. Plasschaert, S. Suliborski, and E.

H. Verdonschot, "Reliability and validity issues of laser fluorescence measurements in occlusal caries diagnosis," *J. Dent.* **30**, 129–134 (2002).
10. A. Lussi, S. Imwinkelried, N. B. Pitts, C. Longbottom, and E. Reich, "Performance and reproducibility of a laser fluorescence system for detection of occlusal caries *in vitro*," *Caries Res.* **33**, 261–266 (1999).
11. X.-Q. Shi, U. Welander, and B. Angmar-Månsson, "Occlusal caries detection with KaVo DIAGNOdent and radiography: an *in vitro* comparison," *Caries Res.* **34**, 151–158 (2000).
12. X.-Q. Shi, S. Tranæus, and B. Angmar-Månsson, "Comparison of QLF and DIAGNOdent for quantification of smooth surface caries," *Caries Res.* **35**, 21–26 (2001).
13. A. Mandelis, L. Nicolaides, C. Feng, and S. H. Abrams, "Novel dental depth profilometric imaging using simultaneous frequency-domain infrared photothermal radiometry and laser luminescence," *Proc. SPIE* **3916**, 130–137 (2000).
14. L. Nicolaides, A. Mandelis, and S. H. Abrams, "Novel dental dynamic depth profilometric imaging using simultaneous frequency-domain infrared photothermal radiometry and laser luminescence," *J. Biomed. Opt.* **5**, 31–39 (2000).
15. A. Mandelis, "Review of progress in theoretical, experimental, and computational investigations in turbid tissue phantoms and human teeth using laser infrared photothermal radiometry," *Proc. SPIE* **4710**, 373–383 (2002).
16. R. J. Jeon, C. Han, A. Mandelis, V. Sanchez, and S. H. Abrams, "Diagnosis of pit and fissure caries using frequency-domain infrared photothermal radiometry and modulated laser luminescence," *Caries Res.* **38**, 497–513 (2004).
17. R. J. Jeon, A. Mandelis, V. Sanchez, and S. H. Abrams, "Non-intrusive, non-contacting frequency-domain photothermal radiometry and luminescence depth profilometry of carious and artificial subsurface lesions in human teeth," *J. Biomed. Opt.* **9**, 804–819 (2004).
18. R. J. Jeon, A. Matvienko, A. Mandelis, S. H. Abrams, B. T. Amaechi, and G. Kullkarni, "Detection of interproximal demineralized lesions on human teeth *in vitro* using frequency-domain Infrared photothermal radiometry and modulated luminescence," *J. Biomed. Opt.* **12**, 034028 (2007).
19. L. Nicolaides, C. Feng, A. Mandelis, and S. H. Abrams, "Quantitative dental measurements by use of simultaneous frequency-domain laser infrared photothermal radiometry and luminescence," *Appl. Opt.* **41**, 768–777 (2002).
20. A. Mandelis, *Diffusion-Wave Fields. Mathematical Methods and Green Functions*, Chap. 2, Springer, New York (2001).
21. A. Mandelis, F. Funak, and M. Munidasa, "Generalized methodology for thermal diffusivity depth profile reconstruction in semi-infinite and finitely thick inhomogeneous solids," *J. Appl. Phys.* **80**, 5570–5578 (1996).
22. B. T. Amaechi, S. M. Higham, and W. M. Edgar, "Factors affecting the development of carious lesions in bovine teeth in vitro," *Arch. Oral Biol.* **43**, 619–628 (1998).
23. B. T. Amaechi and S. M. Higham, "Quantitative light-induced fluorescence: A potential tool for general dental assessment," *J. Biomed. Opt.* **7**, 7–13 (2002).
24. E. de Josselin de Jong, J. J. ten Bosch, and J. Noordman, "Optimised microcomputer guided quantitative microradiography on dental mineralized tissue slices," *Phys. Med. Biol.* **32**, 887–899 (1987).
25. M. N. Braden, "Heat conduction in normal human teeth," *Arch. Oral Biol.* **9**, 479–486 (1964).
26. W. S. Brown, W. A. Dewey, and H. R. Jacobs, "Thermal properties of teeth," *J. Dent. Res.* **49**, 752–755 (1970).
27. A. Matvienko, A. Mandelis, R. J. Jeon, and S. H. Abrams, "Theoretical analysis of coupled diffuse-photon-density and thermal-wave field depth profiles photothermally generated in a layered turbid dental structures," *J. Appl. Phys.*, Special issue on Applied Biophysics (in press).